Wavelength stabilization of a 980-nm semiconductor laser module stabilized with high-power uncooled dual FBG

Yize Huang (黄毅泽)[1], Yi Li (李 毅)[1,2*], Haifang Wang (王海方)[1], Xiaojing Yu (俞晓静)[1], Hu Zhang (张 虎)[1], Wei Zhang (张 伟)[1], Huiqun Zhu (朱慧群)[1,3], Sheng Zhou (周 晟)[1], Ruoxi Sun (孙若曦)[1], and Yuming Zhang (张宇明)[1]

[1]*School of Optical-Electrical and Computer Engineering, University of Shanghai for Science and Technology, Shanghai 200093, China*

[2]*Shanghai Key Laboratory of Modern Optical Systems, Shanghai 200093, China*

[3]*Institute of Thin Films and Nanomaterials, Wuyi University, Jiangmen 529020, China*

[*]*Corresponding author: liyi@usst.edu.cn*

Received July 26, 2010; accepted November 19, 2010; posted online February 21, 2011

An optimized dual fiber Bragg grating (FBG) is proposed for 980-nm semiconductor lasers without thermoelectric coolers to restrict temperature-induced wavelength shift. The mathematical model of the temperature-induced wavelength shift of the laser with the dual FBG is built using the external cavity feedback rate equations. The external cavity parameters are optimized for achieving the stability mode-locking laser output. The spectral characteristics of the dual FBG stabilized laser are measured to range from 0 to 70 °C. The side mode suppression ratio (SMSR) is more than 45 dB, while the full-width at half-maximum (FWHM) is less than 1 nm. The peak wavelength shift is less than 0.1 nm. The dual FBG wavelength shift proportional coefficient is between 0.1086 and 0.4342.

OCIS codes: 140.3425, 140.3480, 140.3570.

doi: 10.3788/COL201109.031403.

High-power wavelength-stabilized 980-nm semiconductor lasers comprise the main pump sources for fiber lasers and erbium-doped fiber amplifiers (EDFAs) in current telecommunications networks[1−5]. Dense wavelength division multiplexing (DWDM) systems with high speed and capacity have been deployed in long-haul and metro networks. EDFAs are efficient optical amplifiers for DWDM systems, and their performance depends on the characteristics of pump lasers, including frequency spectrum, output optical power and polarization state, and so on. The amplifier gain is sensitive to the pump wavelength, which drives the market almost exclusively toward cheap and wavelength-stabilized semiconductor lasers. Conventionally, thermoelectric coolers (TECs) are fixed in semiconductor laser modules to eliminate the output wavelength shift caused by ambient temperature change and current-induced heating. TECs are removed in uncooled laser modules based on fiber Bragg grating (FBG) external cavity stabilization to reduce power consumption, size, and cost. However, it is impossible to avoid a large wavelength detuning between the lasing peak wavelength and the Bragg wavelength at 0–70 °C ambient temperature. Because the dual FBG form, an external cavity as frequency-selective component, the uncooled semiconductor laser can operate within the range of 0–70 °C with an accurate emission wavelength. Contrary to laser modules with the single FBG external cavity semiconductor laser, there is no wavelength detuning in a dual FBG stabilized semiconductor laser[6,7]. In general, the dual FBG external cavity is considered as two filters in series, especially for strong external feedback; however, the dual FBG external cavity should be modeled as a Fabry-Perot (F-P) cavity for weak external feedback because semiconductor lasers are sensitive to the weak external optical feedback. Various dynamics, including instability and chaos, have been reported and observed in this system. Therefore, the investigation of the laser module with the low reflectivity dual FBG based on a F-P external cavity is very important through analysis of the rate equations. Meanwhile, there is a contradiction between the side mode suppression ratio (SMSR) and the output power efficiency in the semiconductor laser module. Relatively high external reflectivity makes the laser achieve high SMSR while decreasing the output power efficiency of the laser. A high-power semiconductor laser is vital to further application. However, suppression of other lasing modes to achieve single longitudinal mode output must greatly reduce the overall output power. When the external length is longer than the coherent length, in which the laser is under the coherence collapse, the laser can operate steadily within the external reflective bandwidth. In this case, the stable output wavelength is achieved. Although the increase of high-frequency noise is caused by the beat-frequency phenomenon under the coherence collapse, numerous modes and their incoherence equalize the low-frequency output power with jumping modes. Therefore, a high-power uncooled dual FBG stabilized 980-nm semiconductor laser module has been proposed to achieve the high SMSR with low output power loss[8−11].

In this letter, the wavelength shift of the semiconductor laser module with dual FBG external cavity is studied through the FBG coupled mode theory and the external cavity feedback rate equations. The characteristics of the F-P external cavity are integrated into the effective external transmittivity ($T_{\rm eff}$), which is substituted into the rate equations to analyze the wavelength shift through the relation between the light and carriers. The active

internal cavity and the passive external cavity are unified into the rate equations, after which the dual FBG external cavity is designed, optimized, assembled, and measured based on the abovementioned study. The experimental results at 0–70 °C prove that the dual FBG can help high-power uncooled 980-nm semiconductor lasers overcome wavelength shift and achieve a stable operating state with good mode-stabilizing and frequency-selective characteristics at the same range of ambient temperature.

Figure 1 shows the structure of the laser module with the dual FBG. The mathematical expressions of the effective external transmittivity of the dual FBG is deduced as:

$$\begin{aligned} T_{\rm eff}(\lambda) &= |t_{\rm g1}|^2 |t_{\rm g2}|^2 / \\ &[1+(1-|t_{\rm g1}|^2)(1-|t_{\rm g2}|^2)+|r_{\rm f}|^2(1-|t_{\rm g1}|^2) \\ &+2\sqrt{(1-|t_{\rm g1}|^2)(1-|t_{\rm g2}|^2)}\cos(-2\beta h+\phi_{\rm r1}+\phi_{\rm r2}) \\ &+2|r_{\rm f}|\sqrt{(1-|t_{\rm g1}|^2)}\cos(-2\beta h+\phi_{\rm r1}) \\ &+2(1-|t_{\rm g1}|^2)|r_{\rm f}|\sqrt{(1-|t_{\rm g2}|^2)}\cos(-2\beta D+2\beta h+\phi_{\rm r2})], \end{aligned} \tag{1}$$

where h is the fiber length between two FBGs; β is the propagation constant; $|t_{\rm g1}|$ and $\phi_{\rm r1}$ are the transmittance of $\rm FBG_1$ and the reflection phase factor of $\rm FBG_1$, respectively; $|t_{\rm g2}|$ and $\phi_{\rm r2}$ are the transmittance of $\rm FBG_2$ and the reflection phase factor of $\rm FBG_2$, respectively; $|r_{\rm f}|$ is the electric field amplitude reflection coefficient of the laser front surface. The Bragg wavelength $\lambda_{\rm B}$ of dual FBG can be obtained by $\min\{T(\lambda_{\rm B})\} = T(\lambda_{\rm B})$ in Eq. (1). The coupling effect of the light in the narrow reflective bandwidth of the dual FBG strengthens the front reflection of the laser.

The resonant cavity of the dual FBG locks the output characteristics of the uncooled semiconductor laser modules. If the length and the feedback wavelength of the dual FBG cavity can meet certain condition: $\delta+\phi_{\rm r1}+\phi_{\rm r2}=2m\pi$, this can lead to harmonic peaks at the central wavelength. In the equation, m is an integer and $\delta = 4\pi nh/\lambda$ is the optical path difference (OPD) caused by the separation of the dual FBG cavity (n is the fiber refractive index). For the dual FBG cavity, when the cavity length and the coupling central wavelength remain unchanged, $\phi_{\rm r1}$ and $\phi_{\rm r2}$ make an increasing impact on the effective bandwidth of the resonant cavity with the decrease of the reflective bandwidth of dual FBG.

When $\rm FBG_1$ and $\rm FBG_2$ are virtually identical, the effective external transmittivity in the case of weak external feedback can be simplified as

$$T_{\rm eff}(\lambda) = \frac{|t_{\rm g}|^4}{1-4(1-|t_{\rm g}|^2)^2\cos(\beta D)\cos(2\phi_r+\beta D-2\beta h)}, \tag{2}$$

where $|t_{\rm g}| = |t_{\rm g1}| = |t_{\rm g2}|$ is the transmittance of the single FBG, and $\phi_{\rm r} = \phi_{\rm r1} = \phi_{\rm r2}$ is the reflection phase factor of the single FBG.

We have described the temperature-induced wavelength shift for the uncooled laser module by a rate equation model expressed by

$$\begin{cases} \dfrac{{\rm d}N}{{\rm d}t} = \dfrac{\eta I}{qV} - (AN+BN^2+CN^3) - v_{\rm g}\dfrac{{\rm d}g}{{\rm d}N}(N-N_{tr})P \\ \dfrac{{\rm d}P}{{\rm d}t} = \Gamma v_{\rm g}\dfrac{{\rm d}g}{{\rm d}N}(N-N_{\rm tr})P - \dfrac{P}{\tau_{\rm P}} + \Gamma\beta_{\rm sp}BN^2 + \rho^2[1-T_{\rm eff}(\lambda)]\dfrac{P}{\tau_m} \end{cases}, \tag{3}$$

where η is the internal quantum efficiency, q is 1.6×10^{-19} C, I is the drive current to the laser, V is the volume of gain medium, $N_{\rm tr}$ is the transparency carrier density, N is the carrier density, ${\rm d}g/{\rm d}N$ is the differential gain, $v_{\rm g}$ is the group velocity of light in the gain medium, P is the photon density, $\tau_{\rm P}$ is the photon lifetime, $\beta_{\rm SP}$ is the spontaneous emission factor, Γ is the confinement factor, A is the nonradiative recombination coeffcient, BN^2 is the rate of spontaneous emission, B is the bimolecular recombination coeffcient, C is the Auger recombination coefficient, ρ is the coupling efficiency between the laser and $\rm FBG_1$, and P/τ_m is the loss rate of photons passing through the dual FBG cavity. Here, τ_m can be described as

$$\tau_m = \frac{2n_d l + 2n(L_{\rm ec}+h)}{c\ln[1/(1-T_{\rm eff})]}, \tag{4}$$

where c is the velocity of light in vacuum, n_d is the refractive index of the semiconductor gain medium, l is the internal cavity length of the laser, and $L_{\rm ec}$ is the external cavity length. The resonance phase condition can be obtained as follows:

$$\frac{4\pi n_d l}{\lambda} + \frac{4\pi n L_{\rm ec}}{\lambda} + \delta + \phi_{\rm r1} + \phi_{\rm r2} = 2m\pi. \tag{5}$$

Then it can yield the mode spacing given by

$$4\pi(n_d l + nD + nh)\frac{|\Delta\lambda|}{\lambda_{\rm B}} + \sum_{i=1}^{2}(|\phi_{\rm ri}(\lambda_{\rm B}) - \phi_{\rm ri}(\lambda_{\rm B}+\Delta\lambda)|) = 2\pi, \tag{6}$$

where D ($D \approx L_{\rm ec}$) is the length between the front surface of the semiconductor laser and $\rm FBG_1$.

Figure 2 shows the numerical simulation results of the carrier density, the photon density and $T_{\rm eff}$ at the dual FBG operating bandwidth. In the case of weak external feedback, the carrier density and the photon density tend to increase in a spiral way as the feedback intensity increases. This indicates that the external longitudinal modes induce the complex laser longitudinal modes.

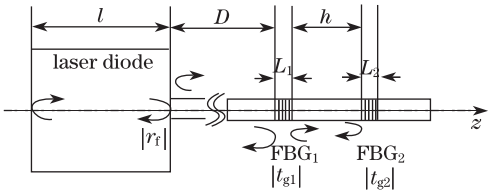

Fig. 1. Schematic diagram of the laser module.

As the feedback intensity increases, the slope of the

carrier density increases. There is a peak reflection at the Bragg wavelength over the dual FBG operating bandwidth. When the current or the lasing wavelength increases, the descending slopes of the carrier density at the two sides of the central wavelength corresponding to the equivalent transmittance intensity of the dual FBG become identical. According to Fig. 2, the higher carrier density corresponds to the slower $T_{\rm eff}$ drop rate. Therefore, there are two lowest transmittance intensities on both sides of the former lowest transmittance intensity at the dual FBG operating bandwidth. The two wavelengths with the lowest transmittance intensities correspond to the highest photon density. If the optical power is unchanged or is relatively stable at the transient stage, the higher photon density shows the average photon energy drops. The long wavelength peak is more easily responded as compared with the short one. Next, there exist four wavelengths with the lowest transmittance intensities in the same manner. Each peak wavelength bifurcation gradually strengthens the inclination to the long wavelength. The bifurcation processes continue until there is no difference in the carrier density between the two sides of the latest peak wavelength. As a result, the whole reflective bandwidth of the dual FBG shifts to the long wavelength as the central wavelength shifts to the long wavelength.

When the laser light passes through the dual FBG, the phase factor leads to smaller lasing mode spacing, and there will be more multi-mode lasing in the dual FBG reflective bandwidth. The laser module with the dual FBG external cavity then produces more spectral lines under the uniform resonance in the dual FBG operating bandwidth. The peak carrier density change is limited, and then wavelength red-shifting is inhibited, which is an effective means of lasing wavelength stability. Among the dynamic longitudinal modes of the different lasing wavelengths, the laser module can instantly produce large amounts of non-coherent photons to suppress the coherent photons, leading multi-mode lasing to the coherence collapse regime. Lasing modes are limited within the reflective bandwidth in order to reduce mode competition under the coherence collapse. The laser can operate more stably under the coherence collapse regime. Usually, the rear surface reflectivity of the laser is 95%, and the front surface reflectivity of the laser is designed based on laser chip length and the external cavity structure[12,13]. For the balance of the output power efficiency and stability of the laser, the range of the front surface reflectivity should be between 0.005 and 0.05. The dual FBG reflectivity is between 3% and 8%. In practice, the best length of the two FBGs should be dependent on the laser properties, such as laser gain spectrum, cavity loss, carrier lifetime, and optical fiber coupling efficiency[14].

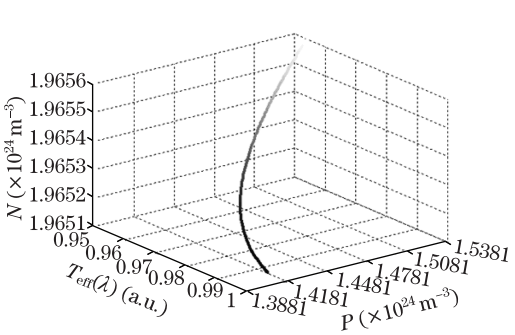

Fig. 2. Numerical simulation results of the rate equation at the dual FBG operating bandwidth.

The effective refractive index of the dual FBG depends on both the lasing wavelength and the carrier density in the gain region. Both the increase in the laser drive current and the increase in ambient temperature T are associated with the increase in carrier density. Given that $n(\lambda, T)/\lambda$ is a constant ($\lambda_{\rm B} = 2n\Lambda$, where Λ is the period of the refractive index), when the laser operates at the stable drive current, we can relate the change in the central wavelength to the change in certain ambient temperature:

$$\mathrm{d}\lambda = \left[\frac{\lambda_0(\partial n/\partial T)}{n_0 - \lambda_0(\partial n/\partial\lambda)}\right]\mathrm{d}T, \tag{7}$$

where λ_0 and n_0 are the peak lasing wavelength and the refractive index without external feedback, respectively.

In Fig. 3, the output peak wavelength of the laser module varies with the change in ambient temperatur. It is shown that the increase of temperature and external reflectivity leads to the peak wavelength red-shifting. Supposing that the temperature-induced wavelength shift from the dual FBG external cavity is dominant in the laser module[15−18], the peak wavelength is almost the same as the Bragg wavelength. In the simplest situation, $\rm FBG_1$ and $\rm FBG_2$ of the dual FBG are the same. The laser module wavelength shift can be expressed as:

$$\Delta\lambda = \kappa\Delta\lambda_{\rm B} = \kappa\xi\lambda_{\rm B}\Delta T, \tag{8}$$

where κ ($0< \kappa <1$) is the dual FBG wavelength shifting proportional coefficient caused by the dual FBG cavity, and ξ is the wavelength shifting coefficient of a single FBG.

Apart from the ambient temperature, there also exists current-induced heating of the laser chip, leading to wavelength shift in the uncooled laser module. However, the effect of current-induced heating plays a minor role here, and it is hardly ever considered because the far field evolution, coupled with nonlinear gain suppression, outweighs the effects of the increase of junction temperature with the increase of drive current[19−25].

Based on the theory above, the parameters of dual FBG are optimized as follows: D = 40 cm, the effective refractive indices of $\rm FBG_1$ and $\rm FBG_2$ $n_1 = n_2$ =1.4545, $\lambda_{\rm B}$ =979.5 nm, the grating lengths of $\rm FBG_1$ and $\rm FBG_2$ $L_1 = L_2$ = 0.19 mm, and h=50 mm.

When the relative humidity was less than 80% and the indoor temperature was 23±1 °C, the power-current

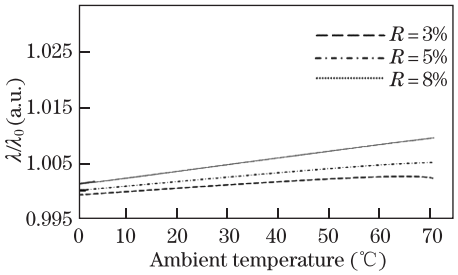

Fig. 3. Calculated T-λ relations with different external reflectivities R.

($L - I$) characteristics and the spectra of the laser module with the dual FBG were measured by optical power meter (OPM) and optical spectrum analyzer (OSA), respectively. These were done in order to test the rationality and accuracy of the optimization design. The laser module and the dual FBG were placed in a temperature-controlled container, where the ambient temperature of 0–70 °C was exactly controlled by proportional integral derivative (PID) controller. The temperature fluctuation was less than 0.5 °C, and the temperature resolution was 0.1 °C. Figure 4 shows the $L - I$ characteristics of the laser module with the dual FBG being linear at the drive current between 30–400 mA.

Figure 5 shows the output spectra of the laser module with the dual FBG when the laser drive current is 400 mA and the ambient temperature of the laser and the dual FBG is from 0 to 70 °C. The peak wavelength shift is less than 0.3 nm, and the SMSR is more than 45 dB. The full-width at half-maximum (FWHM) is less than 1 nm.

Figure 6 shows the output spectra of the laser with the dual FBG when the laser drive current is 400 mA, the dual FBG ambient temperature is 23 °C, and the laser module ambient temperature ranges from 0 to 70 °C. The peak wavelength shift is less than 0.1 nm, and the SMSR is more than 45 dB. The FWHM is less than 1 nm. The results show that the laser module with the dual FBG is almost not affected by the laser ambient temperature and that the wavelength shift of the dual FBG is dominant in the laser module with the dual FBG. The theoretical analysis is almost consistent with the experimental results.

Figure 7 shows the wavelength shift of the laser module with and without the dual FBG at drive currents of 400 and 100 mA, respectively. The wavelength shift of the laser module with the dual FBG is much less than that of the laser module without the dual FBG. At 0–70 °C, the peak wavelengths of the laser module with and without the dual FBG were less than 0.3 nm and larger than 3.5 nm, respectively. Moreover, the laser module with the dual FBG is less affected by the drive current.

Figure 8 shows the $\Delta\lambda/\Delta T$ characteristics of the laser module without the dual FBG and with it at drive currents of 400 and 100 mA and ambient temperature of 0–70 °C, respectively. The curves show that the temperature-induced wavelength shift stability of the laser module with the dual FBG is better and is less affected by the drive current. Compared with $\xi \approx 9.4\times10^{-6}$ °C^{-1} (for the typical germanium-doped silica fiber) in a single FBG, the dual FBG wavelength shift coefficient is less. According to Eq. (8), κ is between 0.1086 and 0.4342 by calculating $\Delta\lambda/\Delta T$ in Fig. 8. The whole results show that the dual FBG can overcome the wavelength shift effectively and achieve a stable operation of the high-power uncooled semiconductor laser.

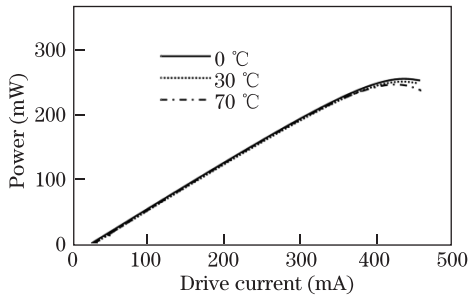

Fig. 4. $L - I$ characteristics of the laser module with the dual FBG at 0, 30, and 70 °C.

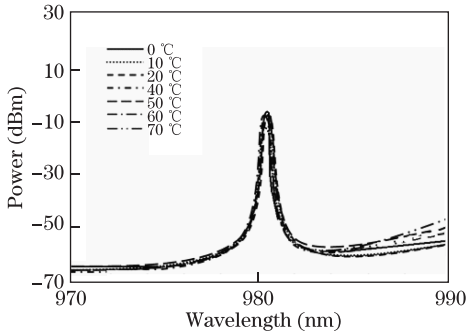

Fig. 5. Spectra of the laser module with the dual FBG when the ambient temperature is from 0 to 70 °C and the laser drive current is 400 mA.

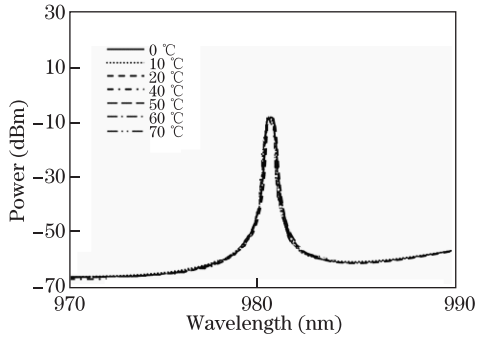

Fig. 6. Spectra of the laser module with the dual FBG when the dual FBG ambient temperature is the room temperature and the laser drive current is 400 mA.

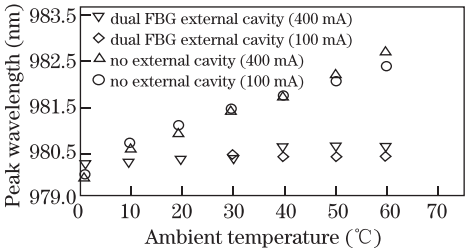

Fig. 7. Wavelength shift of the laser module with and without the dual FBG.

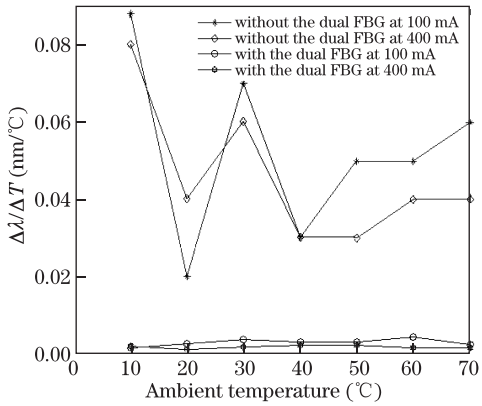

Fig. 8. $\Delta\lambda/\Delta T$ characteristics of the laser module without and with the dual FBG.

In conclusion, through the application of the optimized dual FBG for external stabilization, the wavelength shift stability of the uncooled laser module has been improved in the 0–70 °C operating range. Meanwhile, the mode-stabilizing characteristics are almost not affected by the drive current and the ambient temperature. The wavelength shift of the dual FBG external cavity is dominant in the laser module, which has been proven by the experimental results. In practice, if only the dual FBG can be separated from a heat source or temperature-changing materials, the wavelength shift at 0–70 °C can be less than 0.1 nm. The package of the laser module should be required to reserve certain space for the dual FBG, and the dual FBG should be coated by thermal insulation. The dual FBG can consequently meet the practical requirements of high-power uncooled 980-nm semiconductor lasers.

The work was supported by the National High-Tech Research and Development ("863") Program of China (No. 2006AA03Z348), the Key Program of Science and Technology Research of Shanghai Education Commission (No. 10ZZ94), the Shanghai Leading Academic Discipline Project (No. S30502), and the Shanghai Talents Developing Foundation (No. 014).

References

1. Q. Ma, L. Xia, B. Lu, W. Xiong, Y. Zhang, X. Zhou, and X. Chen, Chin. Opt. Lett. **7,** 46 (2009).
2. S. Hu, Y. Li, Q. Jiang, and B. Wu, Chinese J. Lasers (in Chinese) **35,** 44 (2008).
3. M. Liang, Q. Fang, and Y. Wang, J. Optoelectron. Laser (in Chinese) **12,** 821 (2001).
4. J.-M. Han, S.-J. Baik, J.-Y. Jeong, K. Im, H.-M. Moon, H.-R. Noh, and D.-S. Choi, Opt. Laser Technol. **39,** 313 (2007).
5. S. Feng, O. Xu, S. Lu, X. Mao, T. Ning, and S. Jian, Opt. Laser Technol. **41,** 264 (2009).
6. B. Wu, Y. Li, S. Hu, Q. Jiang, and H. Wang, Chinese J. Lasers (in Chinese) **36,** 799 (2009).
7. D. Bimberg, C. Meuer, M. Lämmlin, S. Liebich, J. Kim, E. Varene, A. Kovsh, I. Krestnikov, and G. Eisenstein, Chin. Opt. Lett. **7,** 266 (2009).
8. C. H. L. Quay, I. Z. Maxwell, and J. A. Hudgings, J. Appl. Phys. **90,** 5856 (2001).
9. I. Fischer, G. H. M. van Tartwijk, A. M. Levine, W. Elsässer, E. Göbel, and D. Lenstra, Phys. Rev. Lett. **76,** 220 (1996).
10. J. S. Lawrence and D. M. Kane, Opt. Commun. **167,** 273 (1999).
11. F. Grillot, B. Thedrez, O. Gauthier-Lafaye, M. F. Martineau, V. Voiriot, J. L. Lafragette, J. L. Gentner, and L. Silvestre, IEEE Photon. Technol. Lett. **15,** 9 (2003).
12. Y. Zhu, H. Mei, T. Zhu, J. Zhang, and S. Yin, Chin. Opt. Lett. **7,** 675 (2009).
13. S. Fukuchi, S.-Y. Ye, and J. Ohtsubo, Opt. Rev. **6,** 365 (1999).
14. S. Hu, Y. Li, Q. Jiang, B. Wu, X. Yu, and H. Wang, Proc. SPIE **7278,** 72781L (2009).
15. K. Li, Z. Zhou, and A. Liu, Chin. Opt. Lett. **7,** 121 (2009).
16. Z. Long, X. Xin, R. Zhou, Z. Zhang, and D. Xu, Chin. Opt. Lett. **8,** 642 (2010).
17. K. Li and Z. Zhou, Chin. Opt. Lett. **7,** 191 (2009).
18. S. Li, X. Liu, Y. Li, S. Yang, and C. Liu, Front. Optoelectron. China **2,** 233 (2009).
19. M. A. Arteaga, M. López-Amo, J. Hernández, K. Koltys, A. Tabaka, H. Thienpont, and K. Panajotov, Opt. Quantum Electron. **40,** 69 (2008).
20. J. M. Noriega, A. Valle, and L. Pesquera, Opt. Quantum Electron. **40,** 119 (2008).
21. M. Achtenhagen, S. Mohrdiek, T. Pliska, N. Matuschek, C. S. Harder, and A. Hardy, IEEE Photon. Technol. Lett. **13,** 415 (2001).
22. X. Qiao, Z. Jia, H. Fu, M. Li, and H. Zhou, Acta Phys. Sin. (in Chinese) **53,** 494 (2004).
23. Z. Jia, X. Qiao, and H. Fu, J. Optoelectron. Laser (in Chinese) **14,** 453 (2003).
24. B. Wu, Y. Li, S. Hu, Q. Jiang, X. Yu, and H. Wang, Proc. SPIE **7135,** 71353A (2008).
25. K. Ni, H. Xu, X. Dong, and Y. Jin, Acta Opt. Sin. (in Chinese) **30,** 2104 (2010).